

## Search for the electromagnetic decay of $\Delta(1232)$ resonance in nuclear matter

A. Badalà,<sup>1</sup> R. Barbera,<sup>1,2</sup> A. Bonasera,<sup>3</sup> M. Gulino,<sup>1,2</sup> A. Palmeri,<sup>1</sup> G. S. Pappalardo,<sup>1</sup> F. Riggi,<sup>1,2</sup> A. C. Russo,<sup>1</sup>  
G. Russo,<sup>1,2</sup> and R. Turrisi<sup>1,2</sup>

<sup>1</sup>*Istituto Nazionale di Fisica Nucleare, Sezione di Catania, Corso Italia, 57-I 95129 Catania, Italy*

<sup>2</sup>*Dipartimento di Fisica dell'Università di Catania, Corso Italia, 57-I 95129 Catania, Italy*

<sup>3</sup>*Istituto Nazionale di Fisica Nucleare, Laboratorio Nazionale del Sud, Via S. Sofia, 44-I 95123 Catania, Italy*

(Received 28 April 1997)

In order to inquire into the existence and significance of non-nucleonic degrees of freedom in the intermediate-energy regime, the production of protons and high-energy photons ( $E_\gamma > 30$  MeV) emitted in the reaction  $^{36}\text{Ar} + ^{27}\text{Al}$  at 95 MeV/nucleon has been studied. The quantitative analysis of the  $(\gamma p)$  invariant-mass and relative-angle distributions shows evidences of  $\Delta(1232)$ -resonance excitation and  $\Delta \rightarrow N\gamma$  decay. Experimental data are in agreement with microscopic theoretical calculations. [S0556-2813(98)02801-5]

PACS number(s): 25.70.Ef, 14.20.Dh, 24.30.Gd

### I. INTRODUCTION

Heavy-ion collisions at bombarding energies ranging from about 100 MeV/nucleon up to a few GeV/nucleon represent a unique tool to study the excitation of non-nucleonic degrees of freedom like baryonic resonances in excited nuclear matter far from ground-state conditions, i.e., outside the usual domain of existing nuclear structure information. Indeed, in a recent paper [1] we have already demonstrated the existence of the elementary *indirect* process  $NN \rightarrow N\Delta \rightarrow NN\pi^0$  in  $^{36}\text{Ar} + ^{27}\text{Al}$  collisions at around 100 MeV/nucleon and we have deduced from experimental data the relative cross section. Notwithstanding  $\Delta \rightarrow N\pi$  is by far the most favored decay channel [branching ratio (B.R.)  $\sim 100\%$  [2]], it is not, however, the best-suited one to study the signals of excitation and propagation of  $\Delta(1232)$  resonance in nuclear matter because of the high distortion introduced by the final-state interactions of pions with the surrounding medium. In this context, the electromagnetic decay  $\Delta \rightarrow N\gamma$  would be, on the contrary, much more appropriate due to the almost complete absence of interaction of photons with nuclear matter. The *free* branching ratio of that decay channel is, however, only  $6 \times 10^{-3}$  [2], and the successful realization of an experiment aimed to the detection of  $\gamma$ 's coming from  $\Delta$  decay has to reckon with the existence of several serious drawbacks: (i) In order not to have contamination from other mechanisms (such as statistical photon emission and/or giant-resonance deexcitation) a lower-energy cutoff of at least 25–30 MeV must be imposed on the data and this strongly reduces the yields, (ii) it is well known that high-energy photons are mostly emitted in the elementary *direct* process  $NN \rightarrow NN\gamma$  so that one has to identify a reasonable ensemble of conditions on the available observables apt to disentangle the *indirect* mechanism from the *direct* one, and (iii) in order to reduce as much as possible the strong background due to photons coming from  $\pi^0$  decays, the bombarding energy should not be much larger than 100 MeV/nucleon and, at the same time, it should not be much smaller than that value because of the consequent reduction of the phase space available for the excitation of the  $\Delta$  resonance.

In spite of this quite discouraging framework, several the-

oretical studies [3–5], based both on statistical [3] and microscopic [4,5] calculations, have drawn the conclusion that  $\gamma$ 's coming from  $\Delta$  electromagnetic decay should be easily observable as they are responsible for the presence of a bump (or, more simply, for a change in the slope) in the photon energy spectrum above  $E_\gamma = 100$  MeV in heavy-ion collisions at bombarding energies between 35 and 200 MeV/nucleon. Since then, several experiments either expressly dedicated [6] or not [7–9] to this issue have measured with a great accuracy the *inclusive* energy spectrum of hard photons emitted in heavy-ion collisions at intermediate energies and no deviation from an exponentially decreasing trend has been observed up to  $E_\gamma \approx 300$  MeV.

In this article we report on the first study of the excitation of the  $\Delta(1232)$  resonance and its electromagnetic decay performed analysing the data of a truly *exclusive* experiment, where high-energy photons emitted in the reactions induced by a 95 MeV/nucleon  $^{36}\text{Ar}$  beam on a  $^{27}\text{Al}$  target (the same reaction studied in Ref. [1]) have been detected in coincidence with protons by a large-area and high-granularity multidetector. For the first time it has been possible to get an estimate of the branching ratio  $\sigma(\Delta \rightarrow N\gamma)/\sigma(\Delta \rightarrow N\pi)$  in nuclear matter and a comparison with its *free* value. This has a great significance since it implicitly allows a quantitative investigation on the weights of two very important processes such as pion reabsorption ( $\pi NN \rightarrow NN$ ) and rescattering ( $\pi N \rightarrow \Delta \rightarrow N\gamma$ ) which can sensibly affect the *in medio* branching ratio with respect to the *free* one.

The paper is organized as follows. The next section is devoted to a description of the experimental setup and particle identification. Experimental results concerning both inclusive and exclusive data are reported in Sec. III. A summary and conclusions are given in Sec. IV.

### II. EXPERIMENTAL SETUP

#### A. Generalities

The experimental setup used basically consisted of the  $\text{BaF}_2$  ball of the MEDEA multidetector. In the experiment described in this paper it was made up of 144 trapezoidal scintillation modules of barium fluoride (20 cm thick) placed

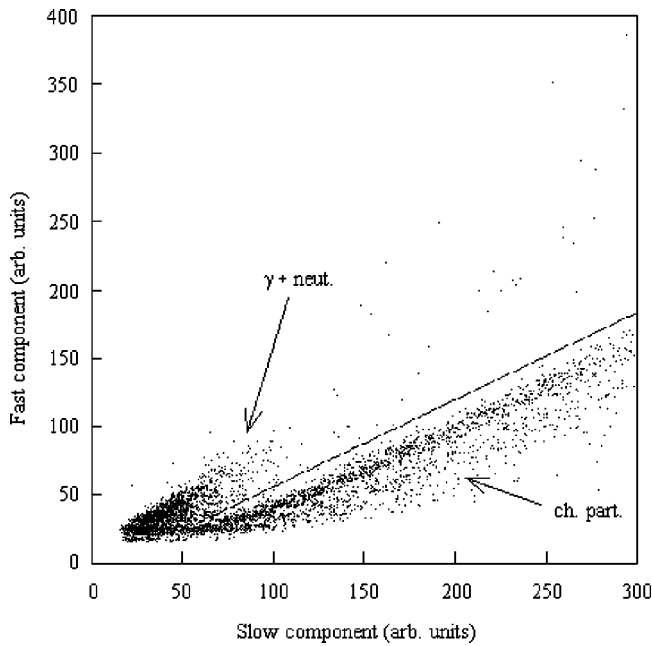


FIG. 1. *Fast-slow* scatter plot relative to an element of the detector.

at 22 cm from the target point and arranged into six rings in order to cover the whole azimuthal angular dynamics between  $\theta=40^\circ$  and  $\theta=140^\circ$  with respect to the beam direction. A very detailed description of this multidetector can be found in Ref. [10].

### B. Particle identification

Particle identification has been accomplished coupling the *fast-slow* technique with the time-of-flight information. Two differently attenuated *slow* signals (*slow1* and *slow2*), belonging to two contiguous regions of the whole energy dynamics, have been separately digitized [10]. Typical *fast-slow* and *time-total* ( $total=slow1+K*slow2$ ) scatter plots relative to an element of the detector are shown in Fig. 1 and Fig. 2, respectively. Photons, which stay above the line drawn in Fig. 1 and in the lower part of Fig. 2, appear very well separated from both neutrons and charged particles. Hydrogen isotopes are clearly visible and fragments with charge  $Z=2$  have been correctly identified and separated. Neutron/photon separation is also shown in Fig. 3 where it is reported the *time-total* scatter plot for those events having *fast-slow* coordinates falling inside the contour drawn in the inset of the figure.

Charged-particle energy calibration has been accomplished using momentum-tagged secondary beams of charged particles (the so-called  $B\rho$  technique in use at the GANIL facility where the experiment was performed). The calibration for low-energy particles ( $E < 25$  MeV) has been slightly scaled in accordance with Ref. [11] in order to take into account quenching effects. The low-energy cutoff is about 10 MeV for protons and about 25 MeV for  $Z=2$  fragments which represent altogether almost all particles detected in the ball. The problem of energy resolution in the  $BaF_2$  ball of MEDEA has been deeply analyzed [12]. Realistic values of (2–4)% [full width at half maximum (FWHM)] have been found in the experiment discussed in

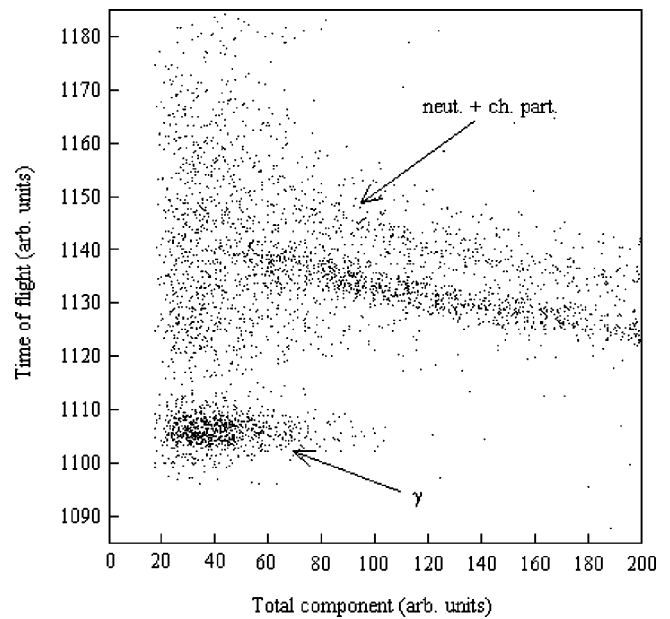


FIG. 2. *Time-total* scatter plot relative to an element of the detector.

the present article which are in agreement with those reported in Ref. [12] (see discussion about Fig. 3 of Ref. [12]).

The  $\gamma$  rays are detected in the  $BaF_2$  ball of MEDEA by means of the calorimetric collection of the electromagnetic showers they induce into the detector material. The determination of the energy and angles of the detected photons is carried out using the following procedure. All modules having a value of the deposited energy different from zero are scanned in order to find the “most-touched” detector (i.e., with the highest value of the deposited energy). Let us call it  $(i_{max}, j_{max})$ , where the index  $i$  ( $i=1,2,\dots,24$ ) is an order parameter running over the elements of one ring and the

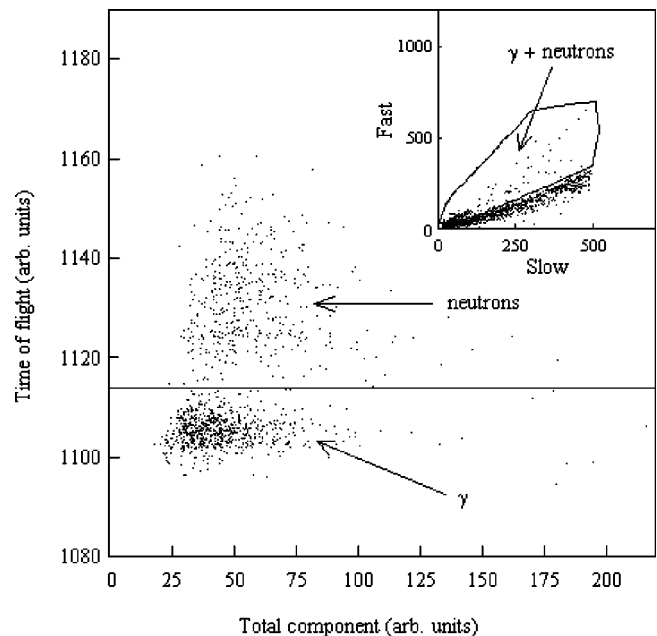


FIG. 3. *Time-total* scatter plot relative to an element of the detector. Only those events having *fast-slow* coordinates falling inside the contour drawn in the inset of the figure have been plotted.

index  $j$  ( $j=1,2,\dots,6$ ) is an order parameter running over the useful rings of the ball. When this detector is found the analysis code looks at all detectors verifying the relation  $(i_{\max}-i)^2+(j_{\max}-j)^2\leq 2$  in order to determine whether or not the electromagnetic shower spreads out in these neighboring modules. If none with a deposited energy greater than its threshold is found, the photon energy is fixed equal to the deposited energy in the central detector and the polar and azimuthal detection angles are uniformly randomized within that detector. Otherwise, as is mostly the case, the energy of the photon-induced shower is obtained by summing over all elements of the array and the photon detection angles are evaluated as the averages of the corresponding (randomized) angles of the single detectors of the array, weighted over the deposited energy in each array element. When the energy and the detection angles of the first shower are determined and the shower multiplicity is greater than 1, the first “most-touched” detector and the involved neighboring modules are excluded from the loop and the program starts again to find a new “most-touched” detector. As has been shown in Refs. [10,13], this kind of procedure minimizes the sideward leakages of the shower (the full side dimension of each detection module is nearly twice the Molière radius of barium fluoride), ensuring a good estimate of the detector response to photons. In order to considerably reduce the background due to neutrons, the condition that the energy deposited in the central detector only must be larger than 20 MeV is also *ex officio* applied to the data.

The energy calibration for photons has been carried out using both a 6.13-MeV  $\gamma$ -ray PuC source and the value of the energy deposited by cosmic rays entering the detectors along their longest side (the energy loss of those minimum ionizing particles is about 6.7 MeV/cm for the BaF<sub>2</sub>). The energy dynamics in which photons have been detected and identified spans from about 20 MeV to 230–250 MeV. The response function of the ball counters of MEDEA to energy-tagged photons has been experimentally determined [14] and successfully compared with full GEANT3 [15] simulations [13] (see next section).

Neutral pions also have been detected in this experiment. They have been recorded in the whole solid angle and in the kinetic energy range between zero and about 120 MeV through the simultaneous detection of the couples of photons coming from their main decay mode ( $\pi^0\rightarrow 2\gamma$ , B.R. = 98.8%). These photons are separated from others pairs by imposing severe conditions on the experimental distributions of the relative angle  $\theta_{12}$  and invariant mass  $m_{\text{inv}}$  as functions of the total energy  $E_1+E_2$  of the two detected photons which are reported, for the <sup>27</sup>Al target, in the upper panel and in the lower panel of Fig. 4, respectively. The cuts drawn in both panels of Fig. 4 select those photons coming from  $\pi^0$  decay and derive from the results of full GEANT3 simulations performed to determine the detector efficiency  $\epsilon(E_\pi, \theta_\pi)$  as a function of the pion kinetic energy and detection angle [13,16] (see next section).

In these last years the capabilities of the MEDEA multidetector as a photon and neutral pion spectrometer have been both extensively simulated [13,14,17,18] and experimentally verified [10,17–20]. The reader is then addressed to those papers for more details.

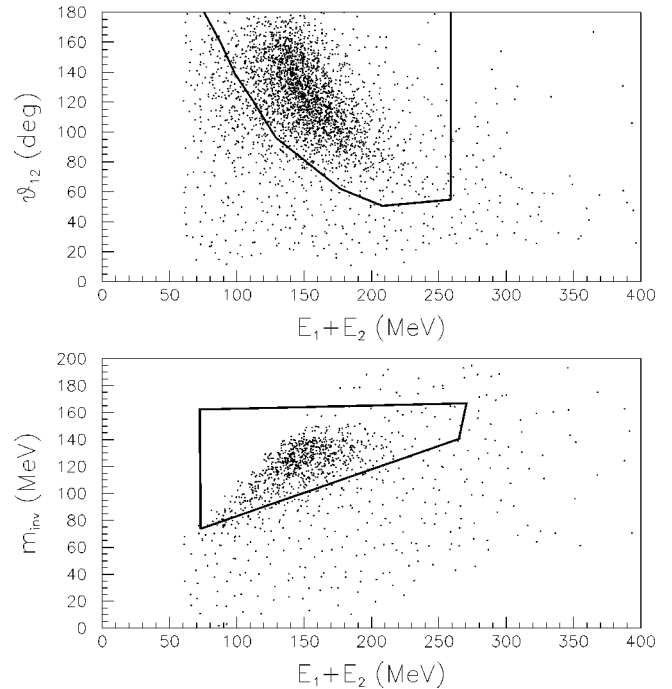


FIG. 4. Relative-angle (upper panel) and invariant mass (lower panel) versus total energy distributions of the pairs of photons detected in the reaction. In both plots, the contours defined by full GEANT3 simulations (see text) select those pairs of photons coming from  $\pi^0$  decay.

### III. RESULTS

#### A. Event selection

In order to reduce as far as possible all sources of background which might have been relevant in the context of this paper, various off-line conditions have been imposed to the data before they could be analyzed.

First of all, both low-energy and small-angle cutoffs of  $E_\gamma=30$  MeV and  $\theta_\gamma=60^\circ$ , respectively, have been applied to all detected photons. The first condition is quite common in the analysis of this kind of experiments and usually prevents the presence of soft photons coming from other mechanisms (evaporation, giant-resonance decay, etc.). The second one has been used to avoid any possible residual contamination of neutrons and/or charged particles (mostly high-energy protons) in the sample of particles identified as photons by means of the technique described in the previous section.

Moreover, only those events where photons have been detected in coincidence with charged particles have been kept for further analysis. This selection criterion has been chosen and imposed to reduce to a negligible amount the otherwise huge background induced by cosmic radiation (see Ref. [17] for all details on that issue).

#### B. Inclusive data

As has been already stated in the Introduction, all so-far-performed experiments either directly aimed or not to the quest for photons coming from the deexcitation of the  $\Delta(1232)$  resonance have dealt (in accordance with theoretical prescriptions) with careful analyses of the shape of the inclusive photon energy spectrum.

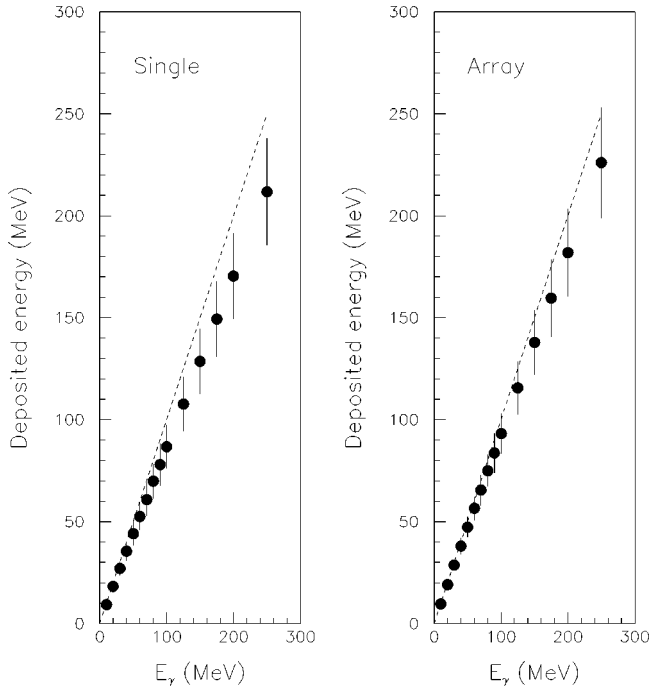


FIG. 5. Mean value of the deposited energy in the central detector (single module of the BaF<sub>2</sub> ball) and in the overall array (see text) including the central one, as a function of the incoming photon energy. The dashed line is the linear (ideal) dependence. Error bars indicate rms deviations.

The same technique has been applied to high-energy photons detected in this experiment. Owing to the importance and delicacy of the problem, however, some comments are in order before showing the results. In fact, when one wants to study the shape of the photon energy spectrum, both a detailed knowledge of the detector response function and a quantitative evaluation of the background induced by photons coming from the  $\pi^0$  main decay mode are mandatory.

Concerning the first argument, which is linked to the efficiency of *finite* real detectors in containing the whole electromagnetic shower induced by the  $\gamma$ 's inside the detector, a full GEANT3 simulation of an exact software replica of the BaF<sub>2</sub> ball of MEDEA has been performed [13,17]. In order to give an idea of the accuracy in the photon energy determination, Figs. 5 and 6 show the mean value and the FWHM of the energy deposited in the detector (and reconstructed in the Monte Carlo simulation) as functions of the incident photon energy. Moreover, in order to give an idea of the accuracy of the knowledge of the detector efficiency for photons, Fig. 7 shows the comparison between a realistic (Boltzmann-like with a slope parameter of 25 MeV) input photon spectrum and that reconstructed after filtering through the detector.

Concerning neutral pion contamination in high-energy photon events, which is the more important the higher is the bombarding energy, it is worth stressing here that it consists of two parts: those events where both photons coming from  $\pi^0$  decay hit the detector and those events where only one photon is detected and the other one gets lost due to geometrical (solid angle coverage) and/or physical (thresholds) inefficiencies of the used detector. The first contribution might be in principle inferred from the ratio between the

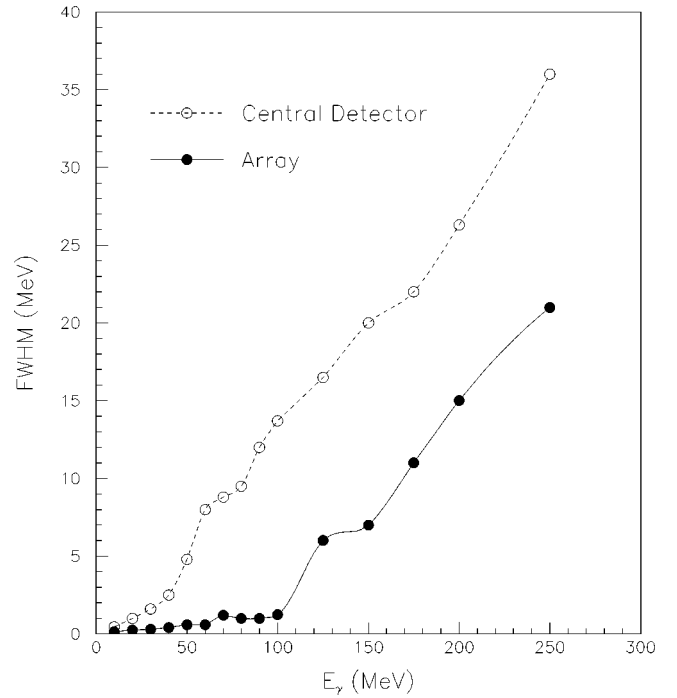


FIG. 6. FWHM of the deposited energy spectrum as a function of the incoming photon energy. The dashed line refers to the case of the single detector and solid line to that of the array (see text).

measured photon and pion cross sections (if one knows the efficiency of the detector to neutral pions) while the second one absolutely needs a computer simulation to be worked out. As part of the same above-cited GEANT3 simulations, the efficiency of the BaF<sub>2</sub> ball of MEDEA to neutral pions has been also evaluated as a function of the pion kinetic energy and emission angle (see Fig. 8). In order to give an idea of

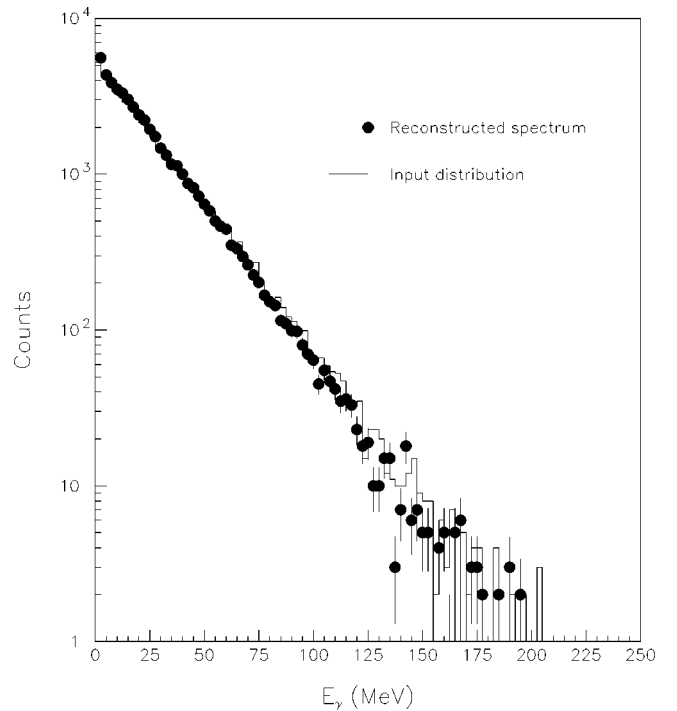


FIG. 7. Comparison between a realistic input photon spectrum and that reconstructed after filtering through the detector.

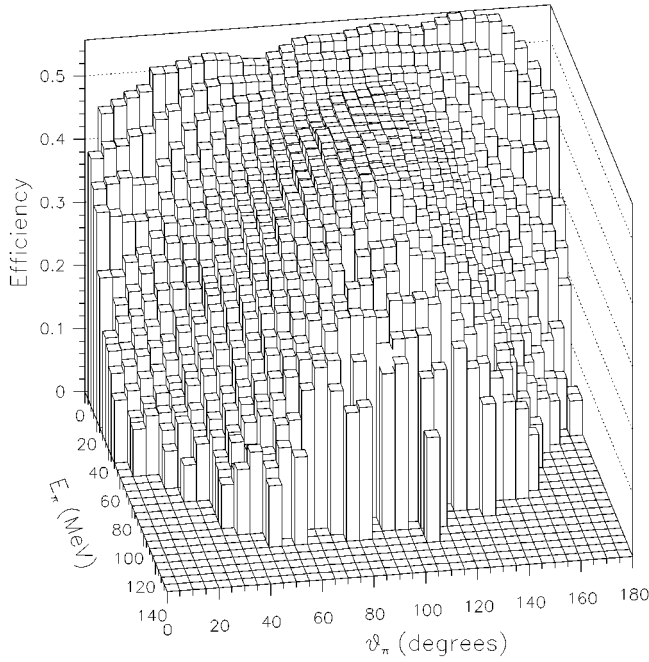


FIG. 8. Detector efficiency for  $\pi^0$ 's as a function of the pion kinetic energy and emission angle.

the accuracy in the knowledge of the detector efficiency for pions, Fig. 9 shows the comparison between a realistic (experimental) input pion spectrum and that reconstructed after filtering through the detector.

For each module of the ball, the number  $N_{\gamma\pi^0}(E_\gamma)$  of photons having a given energy  $E_\gamma$  and coming from  $\pi^0$  decay has been evaluated as

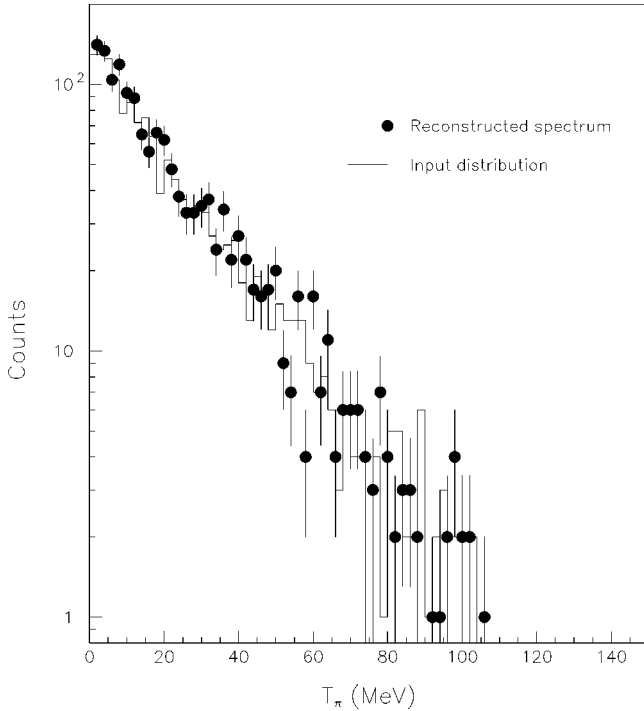


FIG. 9. Comparison between a realistic input pion spectrum and that reconstructed after filtering through the detector.

$$N_{\gamma\pi^0}(E_\gamma) = (N_{1\gamma} + N_{2\gamma}) \frac{N_{\pi^0}^{\text{expt}}}{N_{\pi^0}^{\text{sim}}}, \quad (1)$$

where  $N_{1\gamma}$  is the number of simulated events where only one photon coming from  $\pi^0$  decay is detected,  $N_{2\gamma}$  is the number of simulated events where both photons coming from  $\pi^0$  decay are detected,  $N_{\pi^0}^{\text{expt}}$  is the total number of pions (corrected for the efficiency) detected in the same experimental run of  $\gamma$ 's, and  $N_{\pi^0}^{\text{sim}}$  is the total number of simulated pions. In order to be as realistic as possible in the evaluation of  $N_{1\gamma}$  and  $N_{2\gamma}$  high-energy photons were generated in the phase space according to the results of a moving source analysis [9] which foresees for them an exponential energy spectrum and an isotropic+dipolar angular distribution in their source frame. Neutral pions were generated according to the well-known distribution

$$\left( \frac{d^2N}{d\Omega dE} \right)_{\text{lab}} = pE' \frac{d^2N}{p'^2 dp' d\Omega'}, \quad (2)$$

where

$$E' = \gamma(E - \beta_0 p \cos \theta_{\text{lab}}), \quad (3)$$

$$\gamma = (1 - \beta_0^2)^{-1/2}, \quad (4)$$

and

$$\frac{d^2N}{p'^2 dp' d\Omega'} \propto \frac{1}{4\pi m^3} \frac{e^{-E'/\tau}}{2(\tau/m)^2 K_1(m/\tau) + (\tau/m) K_0(m/\tau)}. \quad (5)$$

$E$ ,  $p$ ,  $E'$ , and  $p'$  are the pion total energies and linear momenta in the laboratory and source frame, respectively.  $\theta_{\text{lab}}$  is the detection angle in the laboratory frame and  $m$  is the rest mass of the neutral pion.  $K_0$  and  $K_1$  are the modified Bessel functions of order 0 and 1, respectively, also known as MacDonald functions [21]. The source parameters are represented by the slope parameter  $\tau$  and the velocity of the source in the laboratory frame,  $\beta_0$ . In our simulations we used  $\beta_0=0.2$  and  $\tau=20$  MeV as typical mean values in agreement with the existing systematics at these bombarding energies.

The comparison between the hard-photon raw energy spectra (open symbols), measured at different polar angles in the laboratory system of reference, and the relative contribution from  $\pi^0$ -decay photons (solid symbols), as obtained from GEANT3 simulations, is reported in Fig. 10. Obviously, one has to calculate, energy by energy and angle by angle, the difference between those spectra to obtain the final (cleaned) photon spectra whose shape is the subject of this subsection.

Cleaned photon energy spectra are reported in Fig. 11 together with the results of the usual moving source analysis. Straight lines drawn in the various panels of Fig. 11 refer in fact to the result of a best-fit procedure simultaneously applied to all photon energies and detection angles with the function

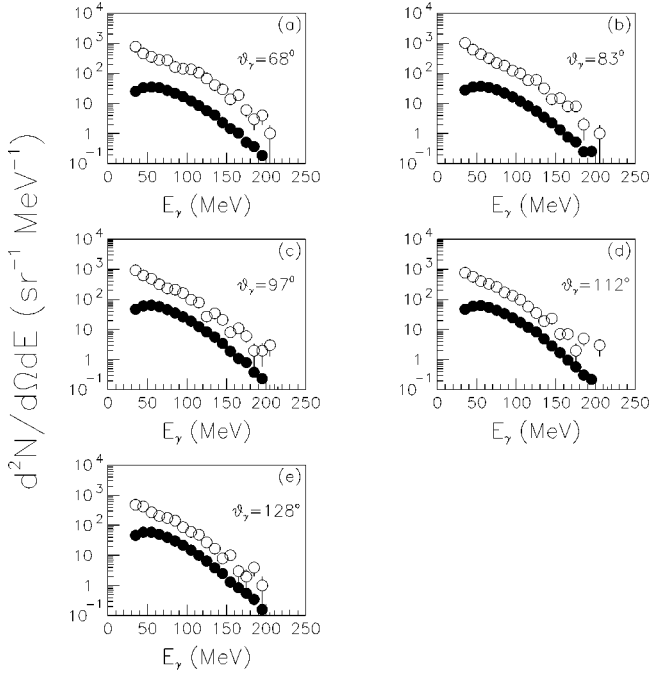


FIG. 10. Comparison between the hard-photon raw energy spectra (open symbols), measured at different polar angles in the laboratory system of reference, and the relative contribution from  $\pi^0$ -decay photons (solid symbols), as obtained from GEANT simulations discussed in the text.

$$\frac{d^2\sigma}{d\Omega dE} = \frac{\sigma_0}{X} \left( 1 - \alpha + \alpha \frac{\sin^2 \theta_{\text{lab}}}{X^2} \right) e^{-XE_{\text{lab}}/E_0}, \quad (6)$$

where

$$X = \frac{(1 - \beta \cos \theta_{\text{lab}})}{\sqrt{1 - \beta^2}}, \quad (7)$$

$\beta$  is the velocity of the source in the laboratory frame,  $E_0$  is the slope parameter,  $\alpha$  is the relative amplitude of the dipolar component of the angular distribution, and  $\sigma_0$  is a normalization factor. The found values of the best-fit parameters are  $\beta = 0.24 \pm 0.05$  (close to the nucleon-nucleon center-of-mass velocity  $\beta_{NN} = 0.22$ ),  $E_0 = (30 \pm 1)$  MeV (in agreement with the existing systematics as a function of the bombarding energy [22]),  $\alpha = 0.2 \pm 0.1$  (the large error is due to the lack, in the data to be fitted, of the photon spectra at the most forward angles in the laboratory), and  $\sigma_0 = (15 \pm 2)$   $\mu\text{b sr}^{-1} \text{MeV}^{-1}$ .

Beyond the physical meaning of the best-fit parameters, what is worth noting here is that up to  $E_\gamma$  larger than 200 MeV the shapes of all photon spectra reported in Fig. 11 are simultaneously well described by a decreasing exponential function. Neither bumps in the spectra nor changes in the slopes are observed in agreement with previously performed experiments [6–9] but in contrast with theoretical expectations [3–5]. In order to support and validate the result of the moving source analysis, experimental photon energy spectra have been also compared with the forecasts of a microscopic theoretical model, based on the solution of Boltzmann-Nordheim-Vlasov (BNV) transport equation, which has been successfully used in the past years to study both hard-photon

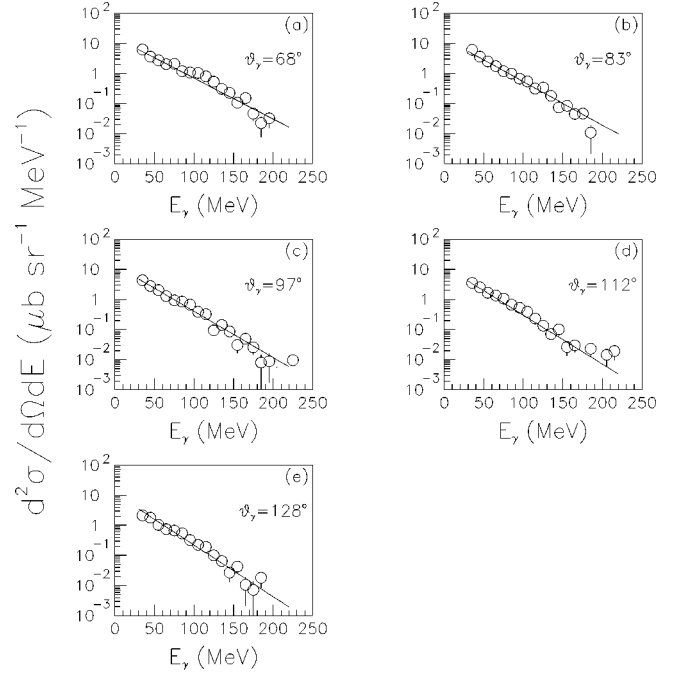


FIG. 11. Hard-photon energy spectra at different laboratory angles measured in the reaction  $^{36}\text{Ar} + ^{27}\text{Al}$  at 95 MeV/nucleon. Data are cleaned of neutral pion contamination. Solid lines refer to the result of the moving source analysis discussed in the text.

and pion production in heavy-ion collisions at intermediate energies. The physical picture underlying the hypotheses of the model is that hard photons are produced in single and incoherent nucleon-nucleon collisions which take place in the overlap volume between the two interacting nuclei at the very first stage of the collision. A new parametrization of the elementary  $np \rightarrow n'p' \gamma$  cross section has been used [23,24]. Indeed, the usual formula which gives the elementary probability  $d^2P_{np\gamma}^{\text{elem}}/dE_\gamma d\Omega_\gamma$  has been modified to take into account the quantal contribution due to *internal radiation* (i.e., bremsstrahlung from the exchanged charged mesons) which is responsible for an increase of the inverse slope parameter of the photon energy spectrum (for all details see Refs. [23,24]). Unlike the model described in Ref. [4], however, no isobaric excitation is explicitly included in the calculation so that we are looking here for any possible disagreement between theory and experiment.

The results of the calculations are compared with the experimental data in Fig. 12 (as in Fig. 11, photon spectra are cleaned of the neutral pion contamination). Apart from a slight overestimation at forward angles and highest energies, the model is able to satisfactorily reproduce both the yields and the shapes of the photon spectra and no room seems to be left over for any other production mechanism.

### C. Exclusive data

Coupling the negative experimental evidences shown in the former subsection with the rest of the existing phenomenology hoarded so far one could be easily tempted to definitely conclude about the nonexistence or the impossibility of detection of photons directly coming from the deexcitation of isobaric resonances created in nuclear matter through nucleon-nucleon collisions. Before drawing any hurried con-

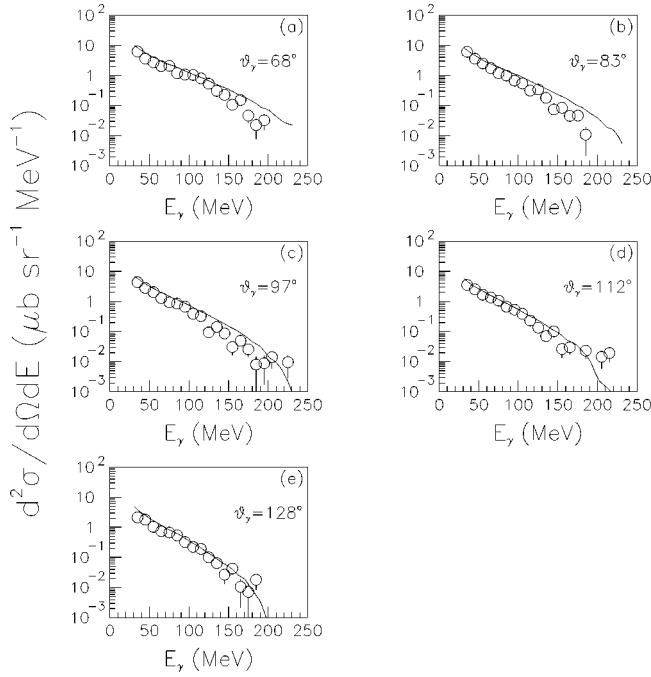


FIG. 12. Comparison between the hard-photon energy spectra and the BNV calculations described in the text.

clusion, however, one should also admit that all investigations conducted up to now have a character strictly *inclusive*. This crucial point deserves a deeper reflection. It is by now well known that high-energy photons are mostly created in single and incoherent nucleon-nucleon collisions  $NN \rightarrow NN\gamma$ . This direct and very rapid contribution to the production cross section largely overwhelms any other channel like the *indirect* one  $NN \rightarrow N\Delta \rightarrow NN\gamma$  which we are interested in in this paper. Furthermore, one also has to take into account that when  $\Delta$ 's are created inside nuclear matter during the collision they almost exclusively decay into a nucleon and a pion, inducing a very large background with respect to the signal one wants to observe. Thus, it should not be so surprising if experimental inclusive energy spectra, which also suffer of an unavoidably finite energy resolution, do not show any signal in the region where it is theoretically expected to be. The situation is not hopeless, however. In fact, if a  $\Delta$  resonance is excited in a nucleon-nucleon collision and then it transforms into a photon and a proton, the final four-momenta of these two particles must be somehow affected by the fact that they come from the decay of a resonant state. Then, a study of kinematical and geometrical correlations between high-energy photons and protons emitted in the same event could provide valuable information about any eventual excitation of non-nucleonic degrees of freedom in nuclear matter at these energies. This is much more than a possibility since in a recent paper [1] we already successfully used this powerful technique of analysis to investigate the  $\Delta \rightarrow N\pi^0$  excitation and decay with the same system at the same bombarding energy.

In the analysis of exclusive  $(\gamma-p)$  events we added the further condition that only one high-energy photon be detected in the event. This cut allows, from one side, to eliminate all two-photon events which have a large probability to come from  $\pi^0$  decay (the detector efficiency of the detection of both photons coming from  $\pi^0$  decay is about twice that of

the detection of only one photon) and, on the other side, to reduce the average proton multiplicity in photon events to  $\nu_p = 1.91 \pm 0.03$ . The question of the value of the proton multiplicity has been already addressed in Ref. [1] but its importance deserves a later comment. When building any  $(\gamma-p)$  correlation function one must, in fact, take care to treat in the same way all the  $\gamma$ -proton couples present in the event because it is not possible to *a priori* decide which proton, if any, comes from  $\Delta$  decay. This means that if  $\nu_p$  protons are present in the event, one has to calculate  $\nu_p$  different values of the given  $(\gamma-p)$  correlation variable for each  $\gamma$ -proton pair and fill the correlation function spectrum  $\nu_p$  times in that event. Thus, if the proton multiplicity in pion events was very large, the combinatorial background introduced would become so large as to invalidate the results.

The first correlation distribution we analyzed was the  $(\gamma-p)$  invariant-mass distribution. For those events where a high-energy photon is detected in coincidence with at least one proton, the  $(\gamma-p)$  invariant-mass distribution has been calculated using the formula

$$m_{\text{inv}} = \sqrt{m_p^2 + 2E_p E_\gamma (1 - \beta_p \cos \theta_{\text{rel}})}, \quad (8)$$

with an obvious meaning of the symbols. In order to be safe from any possible stray angular correlation, proton detection angles (which enter into the calculation of  $\theta_{\text{rel}}$ ) have also been randomized within the angular range covered by the fired detector.

In order to extract a true correlation signal above any combinatorial background level, the same distribution has also been calculated for a sample of so-called *mixed* events which has been generated in accordance with the prescriptions of Ref. [25], i.e., taking the photon from one event and the proton from another randomly chosen event. In order to minimize the statistical error in the *mixed*-event invariant-mass distribution, the total number of *mixed* events is 150 times larger than that of real events. The difference spectrum between the real- and *mixed*-event invariant-mass distributions normalized each other to the same integral is shown in panel (a) of Fig. 13. It is worth emphasizing that both in real and *mixed* distributions the detector efficiency  $\epsilon(\theta_{\text{rel}})$ , as a function of the photon-proton relative angle, has been properly taken into account. From a technical point of view this means that when building the distribution, each event, no matter if it were real or *mixed*, has been included with a weight equal to  $1/\epsilon(\theta_{\text{rel}})$  instead of 1. This efficiency, which is shown in Fig. 14, has been calculated by means of the full GEANT3 simulations discussed above. For protons having an energy above threshold ( $E_{\text{th}} \approx 12$  MeV), the detection efficiency is, for this kind of detector, practically equal to 1 at all angles. This ensures that the difference spectrum reported in Fig. 13 is free from any inefficiency in the coincident photon-proton pair measurement which could not be present in the *mixed* pairs. It is also worth noting that the bin of 20 MeV used has been chosen equal to the worst invariant-mass resolution ( $\sigma$  value) possible in this experiment. The above value has been estimated using the above-cited GEANT3 simulations but it can also be easily calculated starting from the typical experimental resolutions. In fact, considering that the proton mass is not directly measured, the invariant mass reported in Eq. (8) is only a function of the photon energy

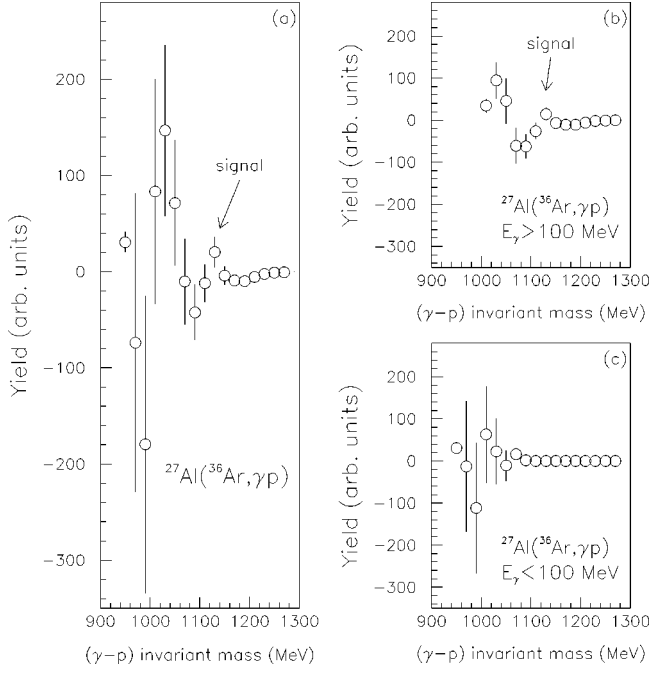


FIG. 13. (a) Difference spectrum between normalized real- and mixed-event  $(\gamma-p)$  invariant-mass distributions. (b) The same as in panel (a) for  $E_\gamma > 100$  MeV. (c) The same as in panel (a) for  $E_\gamma < 100$  MeV. In all panels data are corrected for the relative-angle efficiency (see text).

$E_\gamma$ , of the proton kinetic energy  $T_p$  (the dependence on the velocity  $\beta_p$  can be expressed in terms of  $T_p$  as  $\beta_p = \sqrt{1 - [m_p / (m_p + T_p)]^2}$ ), and of the cosine of the photon-proton relative angle  $\cos\theta_{\text{rel}}$ . Then, the application of the rule of the propagation of errors gives

$$\sigma_{m_{\text{inv}}} = \sqrt{\left(\frac{\partial m_{\text{inv}}}{\partial E_\gamma}\right)^2 \sigma_{E_\gamma}^2 + \left(\frac{\partial m_{\text{inv}}}{\partial T_p}\right)^2 \sigma_{T_p}^2 + \left(\frac{\partial m_{\text{inv}}}{\partial \cos\theta_{\text{rel}}}\right)^2 \sigma_{\cos\theta_{\text{rel}}}^2} \quad (9)$$

with an obvious meaning of the symbols. As a general trend, the invariant-mass resolution increases with the photon and the proton energies. One should keep in mind, however, that the spectra of both particles are exponentially decreasing as a function of the energy and then high energies are less probable. Moreover, as will be more clear in the next section (see Fig. 17), photon and proton energies are anticorrelated so that when one of them is large the other is small. Nevertheless, let us try to calculate the invariant-mass error in the worst case where both  $E_\gamma = 250$  MeV and  $E_p = 250$  MeV, i.e., at the extreme tail of their energy distributions. About the photon-proton relative angle, some comments are in order. Following what is already said above, both photon and proton detection angles are randomized inside the fired detector module. This means that the resolution of the relative angle between those two particles can be easily evaluated from the width of the relative-angle distribution of two particles sent to two modules of MEDEA and whose angles have been correctly randomized within those modules. The result of a very simple Monte Carlo code gives a resolution (FWHM) of about  $6^\circ$  in the whole angular coverage of the detector. Anticipating what will be discussed afterwards (see Fig. 16), photons and protons appear to be correlated at

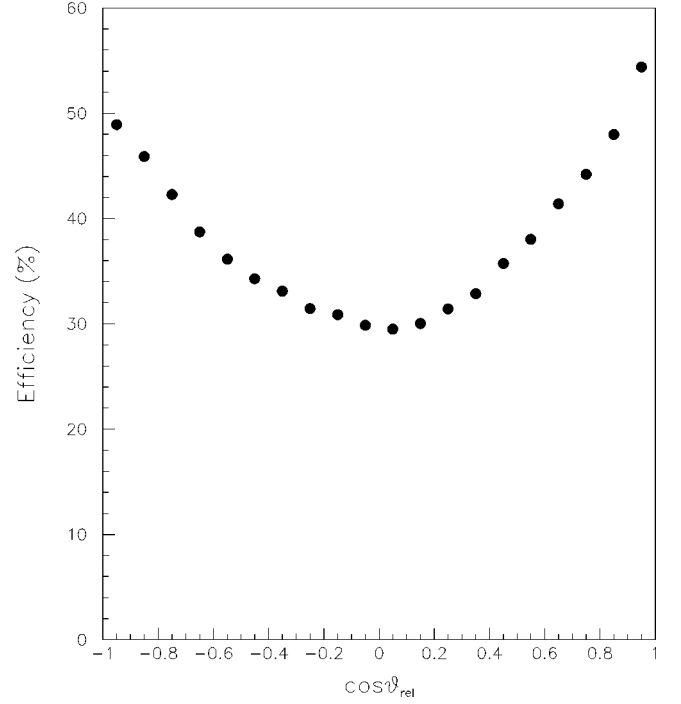


FIG. 14. Detector efficiency as a function of the cosine of the photon-proton relative angle.

around  $\theta_{\text{rel}} \sim 120^\circ$  which gives  $(\text{FWHM})_{\cos\theta_{\text{rel}}} \approx 0.1$ . Then, calculating the derivatives which appear in Eq. (9) and taking into account that (i)  $(\text{FWHM})_\gamma = 20$  MeV (see Fig. 6), (ii)  $(\text{FWHM})_p = 10$  MeV (4% of 250 MeV; see Sec. II B), and (iii)  $(\text{FWHM})_{\cos\theta_{\text{rel}}} = 0.1$ , we get  $\sigma_{m_{\text{inv}}} \approx 18$  MeV.

The distribution plotted in the panel (a) of Fig. 13 shows a correlation around  $m_{\text{inv}} = 1000$  MeV (even if points have large error bars) and a smaller but clearer “negative-positive” signal above  $m_{\text{inv}} = 1060$  MeV (indicated by the arrow in the panel). In order to quantitatively estimate the significance of these two signals with the respect to the null distribution (i.e., no signal at all) we separately applied the  $\chi^2$  test to the points below and above  $m_{\text{inv}} = 1060$  MeV. The results of the test are  $\chi^2/ndf|_{m_{\text{inv}} < 1060 \text{ MeV}} = 1.15$  and  $\chi^2/ndf|_{m_{\text{inv}} > 1060 \text{ MeV}} = 98.12$ , indicating that the first signal is statistically much smaller than how it appears looking at the figure while the second one is absolutely real. The physical interpretation of the first one is quite easy: it is related to those photons emitted in incoherent nucleon-nucleon collisions and it is present here only because of the combination of the proton rest mass with the average values of proton and photon energies above their thresholds ( $m_p + \bar{E}_p + \bar{E}_\gamma \sim 1000$  MeV). The second signal is, on the contrary, quite unexpected and its interpretation is not obvious at first sight. It is, however, placed in the same range of invariant masses where we observed the signal due to the hadronic decay of the  $\Delta$  resonance (see Fig. 1, upper panel, of Ref. [1]). In order to further investigate its origin, we then conditioned the invariant-mass difference spectrum plotted in panel (a) with two separate regions of the photon energy spectrum. Results are reported in panels (b) and (c) of Fig. 13. Panel (b) refers to those photons with an energy larger than 100 MeV (we shall call them “high-energy” photons or HE photons),

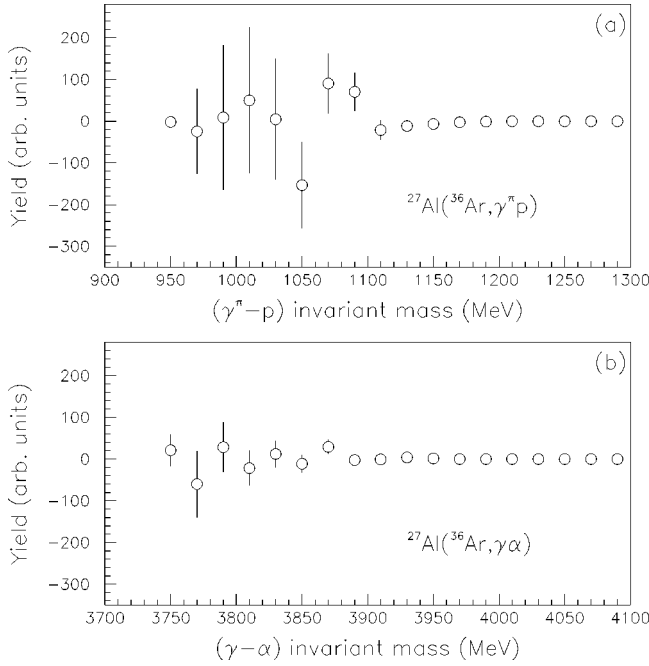


FIG. 15. (a) Difference spectrum between normalized real- and *mixed*-event  $(\gamma^\pi-p)$  invariant-mass distributions (see test for the meaning of  $\gamma^\pi$ ). (b) The same as in panel (a) for  $(\gamma-\alpha)$  events. In all panels data are corrected for the relative-angle efficiency (see text).

while panel (c) refers to those photons having an energy lying between 30 and 100 MeV (we shall call them “low-energy” photons or LE photons). The energy threshold of 100 MeV has been chosen looking at the results of the theoretical calculations performed in Refs. [3–5] where the authors claim that photons coming from the electromagnetic decay of the  $\Delta$  resonance should have an energy greater than 100 MeV in this bombarding energy regime.

For HE photons the correlation around 1000 MeV remains alive while it almost completely disappears for LE photons. This supports the picture that the correlation between photons and protons coming from single nucleon-nucleon collisions should be the more pronounced the smaller is the available phase space for the proton in the elementary collision (similar conclusions have been reached by the authors of Ref. [26], reducing the available phase space for the photon emitted in the elementary nucleon-nucleon collision).

Concerning the most important signal around 1100 MeV, it is still present almost entirely in the case of HE photons while it vanishes in the case of LE photons.

Before drawing any conclusion about the provenance of photons and protons producing the signal observed around  $m_{\text{inv}} \sim 1100$  MeV, one has to show, however, that no experimental bias can invalidate the results shown in Fig. 13. Some considerations to exclude other possible explanations different from the  $\Delta$ -resonance excitation have been already discussed in Ref. [1] and hold for this case too. The reader is then addressed to that paper for more details. Here we only want to report about the investigation on the possible bias due to particle misidentification. We have extracted from experimental data the difference spectra between the real- and *mixed*-event invariant-mass distributions relative to both

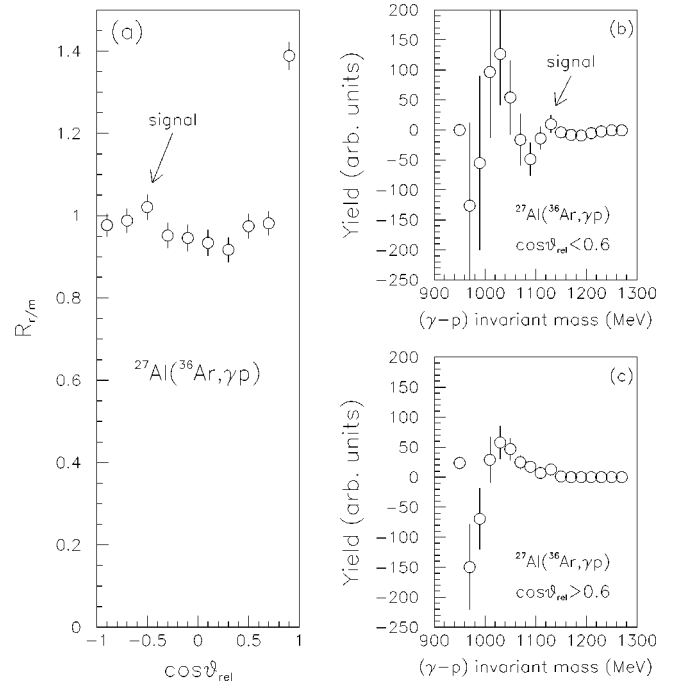


FIG. 16. (a) Ratio between real- and *mixed*-event yields as a function of the cosine of the correlation angle. (b) Difference spectrum between normalized real- and *mixed*-event  $(\gamma-p)$  invariant-mass distributions for  $\cos\theta_{\text{rel}} < 0.6$ . (c) The same as in panel (b) for  $\cos\theta_{\text{rel}} > 0.6$ . In all panels data are corrected for the relative-angle efficiency (see text).

$(\gamma^\pi-p)$  and  $(\gamma-\alpha)$  events. These spectra are plotted in the panel (a) and (b) of Fig. 15, respectively. No signal above the statistical errors is observed. The same  $\chi^2$  test discussed above has been applied to the points of the distributions plotted in panel (a) and (b). The results are  $\chi^2/ndf = 3.77$  for panel-(a) distribution and  $\chi^2/ndf = 1.32$  for panel-(b) distribution.

As has been shown in Ref. [1], the excitation of the  $\Delta$  resonance in nuclear matter can be investigated looking not only at the momentum-energy correlations (as done so far) but also at the geometrical ones. Photons and protons coming from  $\Delta$  decay should indeed evidence definite correlations in their relative-angle distribution. Starting from the measured  $(\gamma-p)$  invariant mass, it is easy to calculate a  $\Delta$  velocity distribution which is peaked at small values, about one-fourth/one-fifth of the speed of the light. This should allow us to expect a preferential *back-to-back* angular correlation even in the laboratory frame between the photon and the proton. In panel (a) of Fig. 16 is plotted the ratio

$$R_{r/m} = \frac{(dN/d\theta_{\text{rel}})_{\text{real events}}}{(dN/d\theta_{\text{rel}})_{\text{mixed events}}} \quad (10)$$

between the normalized  $(\gamma-p)$  real- and *mixed*-event relative-angle distributions. It is worth noting that a bin larger than the experimental resolution of  $\theta_{\text{rel}}$  (see above) has been used and that the relative-angle efficiency has been taken into account.

The distribution is strongly peaked at small relative angles, where the contribution of photons coming from incoherent nucleon-nucleon collisions is mostly expected, but it

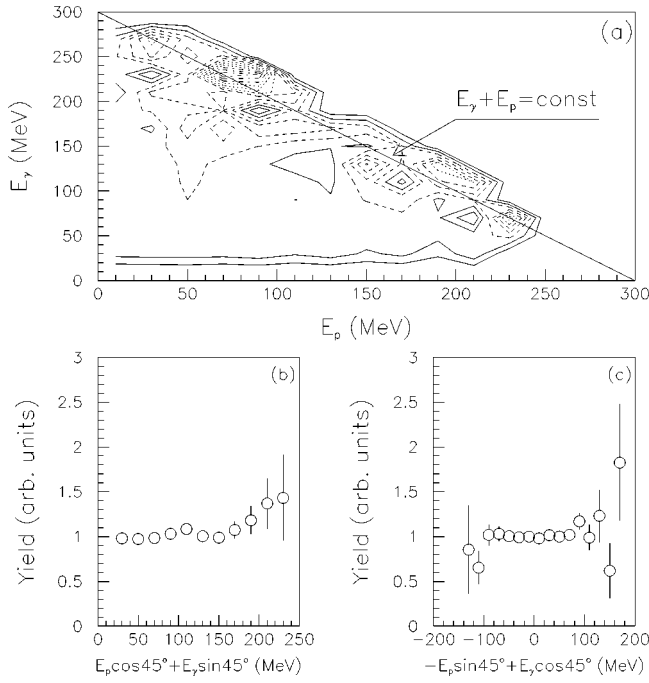


FIG. 17. (a) Bidimensional distribution of the photon energy vs the proton kinetic energy. The solid line indicates the locus of the points for which  $E_\gamma + E_p = \text{const}$ . (b) Projection of the distribution plotted in panel (a) on an axis perpendicular to the axis  $E_\gamma + E_p = \text{const}$ . (c) Projection of the distribution plotted in panel (a) on the axis  $E_\gamma + E_p = \text{const}$ .

also shows a signal at much larger relative angles (indicated by the arrow in the panel). In order to disentangle the contribution of direct photons from that due to *indirect* ones, we conditioned the invariant-mass difference spectrum plotted in panel (a) of Fig. 13 with two separate regions of the  $(\gamma-p)$  relative-angle distribution. Results are reported in panels (b) and (c) of Fig. 16. Panel (b) refers to those photon-proton pairs for which  $\cos\theta_{\text{rel}} < 0.6$  (we shall call them ‘‘large-angle’’ pairs or LA pairs), while panel (c) refers to those photon-proton pairs having  $\cos\theta_{\text{rel}} > 0.6$  (we shall call them ‘‘small-angle’’ pairs or SA pairs). In the case of LA pairs the signal around  $m_{\text{inv}} = 1100$  MeV is still present, while in the case of SA pairs it completely disappears.

All experimental evidence described so far indicates that we are really observing the excitation of the  $\Delta$  resonance in nuclear matter and its subsequent electromagnetic decay. Then the energy of the photon and that of the proton cannot be barely independent one from each other (since both particles come from the decay of a resonant state) and a correlation signal should be visible in the  $(E_p - E_\gamma)$  plane. In fact, if two particles (let us call them 1 and 2) come from the binary decay of a resonant state, their energies must define a locus in the  $(E_1 - E_2)$  plane. This locus is the straight line  $E_1 + E_2 = \text{const}$  if the parent state is (almost) at rest in the laboratory reference frame. As has been already said above, the  $\Delta$  velocity distribution is peaked at small values so that one should observe a correlation all around the locus  $E_p + E_\gamma = \text{const}$  independently of the photon energy and photon-proton relative angle. Actually, the real situation is not so simple due to the presence of the huge background coming from uncorrelated photons and protons and a comparative analysis of real- and *mixed*-event distributions is mandatory.

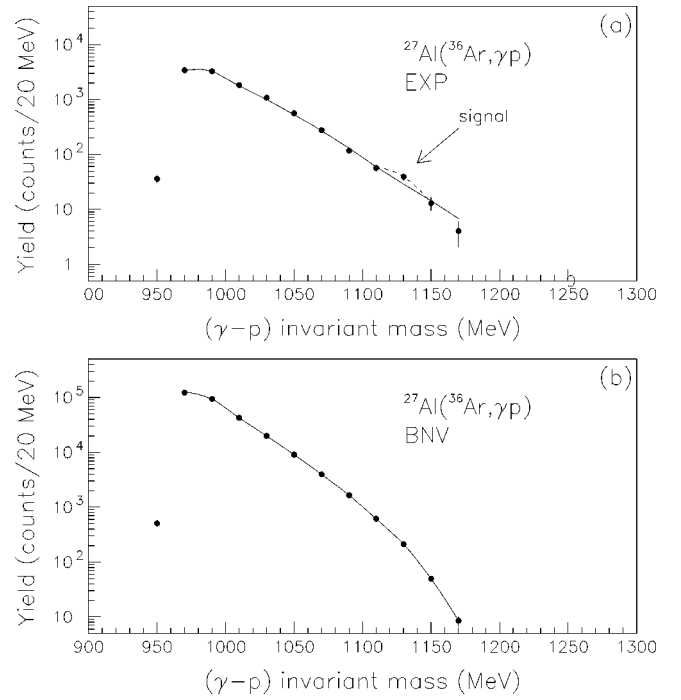


FIG. 18. (a) Experimental  $(\gamma-p)$  invariant-mass distribution relative to real events. (b)  $(\gamma-p)$  invariant-mass distribution relative to those events generated by the BNV code described in the text. In panel (a) the solid line is relative to the *mixed*-event distribution while dashed line is drawn to guide the eye. In panel (b) the solid line is drawn to guide the eye.

Panel (a) of Fig. 17 shows the ratio between the real- and *mixed*-event bidimensional distributions of the photon energy vs the proton kinetic energy. Indeed, a clear correlation signal emerges all around the locus  $E_p + E_\gamma = \text{const}$ , which is drawn in the figure as a straight line. The existence of the correlation signal and its constant presence over all the photon and proton energy ranges are confirmed by the shapes of the projections of the distribution plotted in panel (a) on an axis perpendicular to the axis  $E_p + E_\gamma = \text{const}$  and on the axis  $E_p + E_\gamma = \text{const}$  itself, which are reported in panel (b) and (c) of Fig. 17, respectively.

In the previous subsection we have demonstrated that *inclusive* observables, such as the photon energy spectra at various polar angles in the laboratory frame, do not show (contrarily to the theoretical expectations) any signal due to the excitation of baryonic resonances in nuclear matter and they have been well reproduced by the BNV calculations which do not contain such non-nucleonic degrees of freedom. In this subsection, on the contrary, *exclusive* observables, such as the  $(\gamma-p)$  invariant-mass and relative-angle distributions, have shown clear indications of the excitation of the  $\Delta$  resonance and its electromagnetic decay. Then, it should be very interesting and instructive to compare *exclusive* data with the results of the same BNV model. To this end we improved the BNV code in order to generate a statistically adequate sample of events, each containing a proton having an energy larger than the experimental threshold and a more-than-30-MeV photon which were then filtered through a software replica of the real detector. The comparison between the experimental real-event  $(\gamma-p)$  invariant-mass distribution (upper panel) and that calculated by the

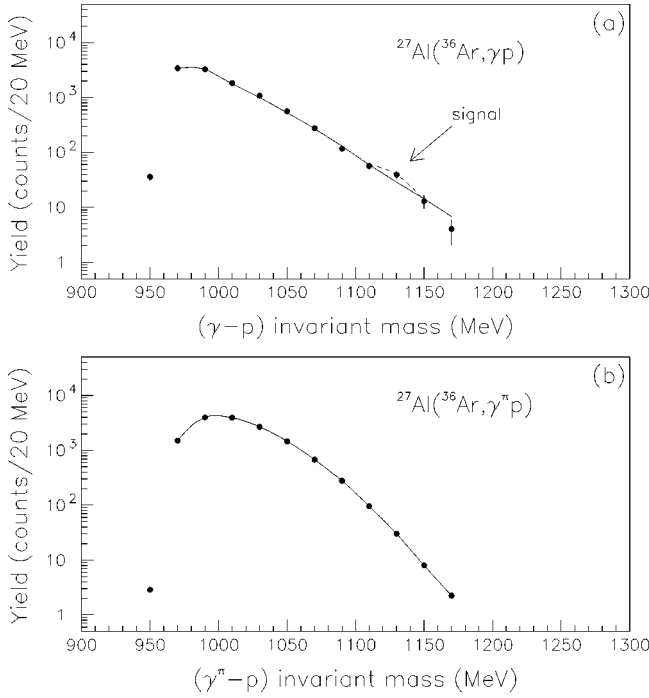


FIG. 19. (a) Experimental  $(\gamma-p)$  invariant-mass distribution relative to real events. (b) Experimental  $(\gamma^\pi-p)$  invariant-mass distribution relative to real events (see test for the meaning of  $\gamma^\pi$ ). In both panels solid lines are relative to the corresponding *mixed-event* distributions. The dashed line in panel (a) is drawn to guide the eye.

BNV model (lower panel) is reported in Fig. 18. In panel (a) the solid line is relative to the *mixed-event* distribution normalized at  $m_{\text{inv}}=970$  MeV (far from the correlation region). The proton multiplicity in the BNV events is, by construction, strictly equal to 1 so that there is no effect of the combinatorial background and the comparison with the experimental data can obviously be only qualitative. Nevertheless, the experimental distribution clearly shows the presence of a signal (a shoulder in the range  $m_{\text{inv}}=1100-1150$  MeV) which is completely absent in the theoretical distribution. This signal is not due to any experimental bias and it is characteristic of  $(\gamma-p)$  events as is demonstrated in Fig. 19 where the same experimental real-event  $(\gamma-p)$  invariant-mass distribution (upper panel) is compared with the  $(\gamma^\pi-p)$  one (lower panel) where no signal is observable. In both panels solid lines are relative to the corresponding *mixed-event* distributions normalized at  $m_{\text{inv}}=970$  MeV. The comparison between the experimental real-event  $(\gamma-p)$  relative-angle distributions (upper panels) and those calculated by the BNV model (lower panels) is reported in Fig. 20. LE photons (left panels) and HE photons (right panels) are separately compared. Experimental distributions show the presence of a signal at large relative angles whose size increases as a function of the photon energy. The signal is completely absent in the BNV distributions independently of the photon energy. Both in the case of LE photons and HE photons, on the contrary, the strong small-relative-angle component relative to direct photons coming from incoherent nucleon-nucleon collisions is well reproduced by the model.

The coupling of the results on the electromagnetic decay of the  $\Delta$  resonance, reported in this paper, with those relative

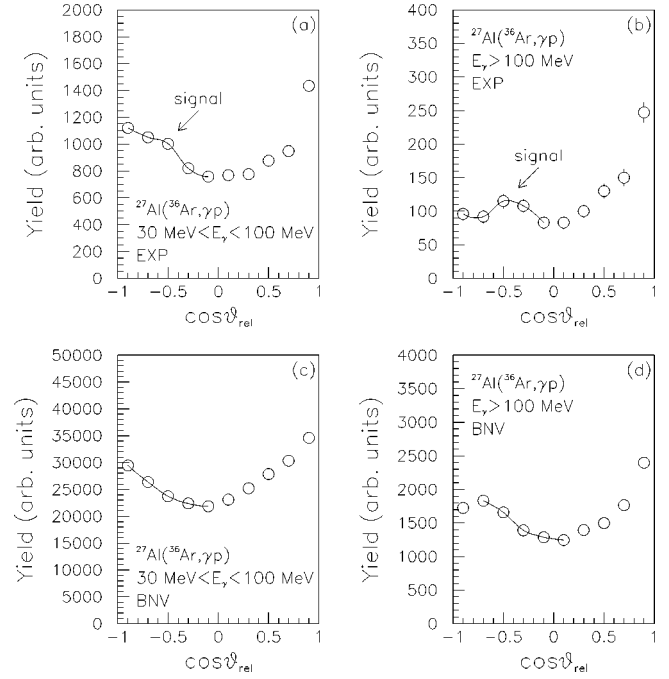


FIG. 20. (a) Ratio between experimental real- and *mixed-event* yields as a function of the cosine of the correlation angle for  $E_\gamma < 100$  MeV. (b) The same as in panel (a) for  $E_\gamma > 100$  MeV. (c) The same as in panel (a) for BNV events. (d) The same as in panel (b) for BNV events.

to the hadronic decay of the  $\Delta$  resonance, performed in Ref. [1], offers the unique possibility to evaluate the *in medio* branching ratio  $\text{B.R.} \equiv \sigma_{\Delta \rightarrow N\gamma} / \sigma_{\Delta \rightarrow N\pi}$ . Moreover, comparing it with the *free* value equal to  $6 \times 10^{-3}$ , one can have a global quantitative estimation of the pion reabsorption and rescattering effects inside excited nuclear matter. The measured cross section of the *indirect* channel  $NN \rightarrow N\Delta \rightarrow NN\gamma$  has been evaluated here using the formula

$$\sigma_{\Delta \rightarrow N\gamma} = \frac{\sigma_\gamma}{N_\gamma} N_{\Delta \rightarrow N\gamma}, \quad (11)$$

where  $\sigma_\gamma$  is the total photon production cross section,  $N_\gamma$  is the total number of high-energy photons detected, and  $N_{\Delta \rightarrow N\gamma}$  is the total number of high-energy photons coming from the *indirect* channel. This latter quantity has been evaluated normalizing the real- and the *mixed-event*  $(\gamma-p)$  invariant-mass distributions (which is a very good approximation of the combinatorial background) in the region  $m_{\text{inv}} < 1000$  MeV (where no correlation is observed) and then calculating the integral of the difference spectrum in the interval  $m_{\text{inv}}=1050-1150$  MeV. The final result is  $\sigma_{\Delta \rightarrow N\gamma} = (1.6 \pm 1.2) \mu\text{b}$  which, together with the value reported in Ref. [1] for  $\sigma_{\Delta \rightarrow N\pi}$ , gives  $\text{B.R.} = (7.6 \pm 5.9) \times 10^{-2}$ . Taking into account the fact that in this experiment photons and neutral pions have been detected in different angular ranges, this value of the branching ratio, although affected by a rather large error bar, is compatible with that of  $3.3 \times 10^{-2}$  foreseen in Ref. [4].

#### IV. SUMMARY AND CONCLUSIONS

A comparative analysis of inclusive and exclusive data on high-energy-photon production in heavy-ion collisions at intermediate energies has been successfully conducted in order to investigate the excitation of non-nucleonic degrees of freedom in excited nuclear matter which is a very delicate topic in this field of nuclear physics.

Indeed, the study of both kinematical (invariant-mass) and geometrical (relative-angle) observables has allowed us to claim the first clear and direct observation of the elementary *indirect* process  $NN \rightarrow N\Delta \rightarrow NN\gamma$  whose revealability was predicted several years ago by theoretical calculations but never proved in any of the *inclusive* experiments realized so far. Together with those reported in Ref. [1] about the el-

ementary *indirect* process  $NN \rightarrow N\Delta \rightarrow NN\pi^0$  (for the same system at the same bombarding energy), the results presented in this paper represent the up-to-date most complete information about the excitation and decay of the  $\Delta(1232)$  resonance in nuclear matter in this energy regime.

The first estimation of the *in medio* branching ratio  $\sigma_{\Delta \rightarrow N\gamma} / \sigma_{\Delta \rightarrow N\pi}$  has been also performed and the result is in agreement with the prediction of a microscopic theoretical calculation.

Explicitly dedicated experiments could in the future take advantage of these results to investigate in a more complete and quantitative manner on the phenomena of pion reabsorption and rescattering in nuclear matter far from the ground state as well as on the space-time evolution of the reaction.

- 
- [1] A. Badalà, R. Barbera, A. Bonasera, A. Palmeri, G. S. Pappalardo, F. Riggi, A. C. Russo, G. Russo, and R. Turrisi, *Phys. Rev. C* **54**, R2138 (1996).
- [2] M. Aguilar-Benitez *et al.*, *Phys. Rev. D* **50**, 1173 (1994).
- [3] M. Prakash, P. Braun-Munzinger, J. Stachel, and N. Alamanos, *Phys. Rev. C* **37**, 1959 (1988).
- [4] W. Bauer and G. F. Bertsch, *Phys. Lett. B* **229**, 16 (1989).
- [5] A. Bonasera, G. F. Burgio, F. Gulminelli, and H. H. Wolter, *Nuovo Cimento A* **103**, 309 (1990).
- [6] J. Clayton, J. Stevenson, W. Benenson, D. Krofchek, D. J. Morrissey, T. K. Murakami, and J. S. Winfield, *Phys. Rev. C* **42**, 1009 (1990).
- [7] J. Stevenson *et al.*, *Phys. Rev. Lett.* **57**, 555 (1986).
- [8] M. Kwato Njock, M. Maurel, E. Monnard, H. Nifenecker, P. Perrin, J. A. Pinston, F. Schussler, and Y. Schutz, *Nucl. Phys. A* **489**, 368 (1988).
- [9] A. Schubert *et al.*, *Phys. Rev. Lett.* **72**, 1608 (1994).
- [10] E. Migneco *et al.*, *Nucl. Instrum. Methods Phys. Res. A* **314**, 31 (1992).
- [11] T. Murakami, J. Kasagi, H. Tachibanaki, K. Yoshida, Y. Shibata, T. Nakagawa, M. Ogihara, S. M. Lee, T. Kubo, and T. Motobayashi, *Nucl. Instrum. Methods Phys. Res. A* **253**, 163 (1986).
- [12] A. Del Zoppo *et al.*, *Nucl. Instrum. Methods Phys. Res. A* **327**, 363 (1993).
- [13] A. Badalà, R. Barbera, A. Palmeri, G. S. Pappalardo, F. Riggi, and A. C. Russo, *Nucl. Instrum. Methods Phys. Res. A* **306**, 283 (1991).
- [14] G. Bellia *et al.*, *Nucl. Instrum. Methods Phys. Res. A* **329**, 173 (1994).
- [15] CERN Application Software Group, *GEANT: Detector Description and Simulation Tool* (CERN, Geneva, 1993); CERN Program Library Long Writeups W5013.
- [16] A. Badalà, R. Barbera, A. Palmeri, G. S. Pappalardo, F. Riggi, A. C. Russo, G. Russo, and R. Turrisi, *Phys. Rev. C* **55**, 2506 (1997).
- [17] A. Badalà, R. Barbera, A. Palmeri, G. S. Pappalardo, F. Riggi, A. C. Russo, G. Russo, and R. Turrisi, *Nucl. Instrum. Methods Phys. Res. A* **351**, 387 (1994).
- [18] A. Badalà, R. Barbera, A. Palmeri, G. S. Pappalardo, F. Riggi, A. C. Russo, G. Russo, and R. Turrisi, *Nucl. Instrum. Methods Phys. Res. A* **357**, 443 (1995).
- [19] A. Badalà *et al.*, *Phys. Rev. C* **48**, 2350 (1993).
- [20] A. Badalà *et al.*, *Phys. Rev. C* **47**, 231 (1993).
- [21] *Handbook of Mathematical Functions*, edited by M. Abramowitz and I. A. Stegun (Dover, New York, 1972).
- [22] W. Cassing, V. Metag, U. Mosel, and K. Niita, *Phys. Rep.* **188**, 363 (1990).
- [23] G. Russo, *Phys. Rev. C* **48**, 2926 (1993).
- [24] G. Russo, *Nucl. Phys. A* **575**, 449 (1994).
- [25] D. Drijard, H. G. Fischer, and T. Nakada, *Nucl. Instrum. Methods Phys. Res. A* **225**, 367 (1984).
- [26] P. Sapienza *et al.*, *Phys. Rev. Lett.* **73**, 1769 (1994).